



Continuous-wave 1550 nm operated terahertz system using ErAs:In(Al)GaAs photoconductors with 52 dB dynamic range at 1 THz

A. D. J. FERNANDEZ OLVERA,¹ H. LU,² A. C. GOSSARD,³ AND S. PREU^{1,*}

¹*Terahertz Systems Technology, Dept. of Electrical Engineering and Information Technology, Technische Universität Darmstadt, Merckstr. 25, D-64283 Darmstadt, Germany*

²*College of Engineering and Applied Sciences, Nanjing University, China*

³*Materials Dept., University of California, Santa Barbara, USA*

*preu@imp.tu-darmstadt.de

Abstract: Telecom-wavelength compatible photoconductors benefit strongly from the large amount and affordability of telecom lasers and components but there are demanding requirements on material development. We demonstrate continuous-wave (CW) photomixing with a setup that only uses ErAs:In(Al)GaAs devices with a peak dynamic range (DNR) of 78 dB and a bandwidth of ~3.65 THz at an integration time of 300 ms and only 26 mW laser power on each device. The ErAs:InGaAs receiver further features a factor of two lower noise equivalent power (NEP) than a state-of-the-art photoconductor, despite an antenna mismatch.

© 2017 Optical Society of America under the terms of the [OSA Open Access Publishing Agreement](#)

OCIS codes: (160.5140) Photoconductive materials; (040.2235) Far infrared or terahertz; (230.0040) Detectors; (040.5150) Photoconductivity.

References and links

1. U. R. Pfeiffer, Y. Zhao, J. Grzyb, R. Al Hadi, N. Sarmah, W. Förster, H. Rucker, and B. Heinemann, "A 0.53 THz reconfigurable source module with up to 1 mW radiated power for diffuse illumination in terahertz imaging applications," *IEEE J. Solid-State Circuits* **49**, 2938–2950 (2014).
2. B. Heinemann, H. Rucker, R. Barth, F. Bärwolf, J. Drews, G. Fischer, A. Fox, O. Fursenko, T. Grabolla, F. Herzel, J. Katzer, J. Korn, A. Krüger, P. Kulse, T. Lenke, M. Lisker, S. Marschmeyer, A. Scheit, D. Schmidt, J. Schmidt, M.A. Schubert, A. Trusch, C. Wipf, and D. Wolansky, "SiGe HBT with f_x/f_{max} of 505 GHz/720 GHz," in "Electron Devices Meeting (IEDM), 2016 IEEE International," (IEEE, 2016), pp. 1–3.
3. J. C. Rode, H.-W. Chiang, P. Choudhary, V. Jain, B. J. Thibeault, W. J. Mitchell, M. J. Rodwell, M. Urteaga, D. Loubychev, A. Snyder, Y. Wu, J. M. Fastenau, and A. W. K. Liu, "Indium phosphide heterobipolar transistor technology beyond 1-THz bandwidth," *IEEE Trans. Electron Devices* **62**, 2779–2785 (2015).
4. G. Scalari, C. Walther, M. Fischer, R. Terazzi, H. Beere, D. Ritchie, and J. Faist, "THz and sub-THz quantum cascade lasers," *Laser and Photonics Reviews* **3**, 45–66 (2009).
5. S. Preu, G. H. Döhler, S. Malzer, L. Wang, and A. C. Gossard, "Tunable, continuous-wave terahertz photomixer sources and applications," *J. Appl. Phys.* **109**, 061301 (2011).
6. T. Göbel, D. Stanze, B. Globisch, R. J. Dietz, H. Roehle, and M. Schell, "Telecom technology based continuous wave terahertz photomixing system with 105 decibel signal-to-noise ratio and 3.5 terahertz bandwidth," *Optics Lett.* **38**, 4197–4199 (2013).
7. A. R. Criado, C. de Dios, G. H. Döhler, S. Preu, S. Malzer, S. Bauerschmidt, H. Lu, A. C. Gossard, and P. Acedo, "Ultra-narrow linewidth CW sub-THz generation using GS based OFCG and n-i-pn-i-p superlattice photomixers," *Electron. Lett.* **48**, 1425–1426 (2012).
8. E. R. Brown, "THz generation by photomixing in ultrafast photoconductors," *Int. J. High Speed Electron. and Systems* **13**, 497–545 (2003).
9. G. Carpintero, L. Garcia-Munoz, H. Hartnagel, S. Preu, and A. Räisänen, *Semiconductor THz Technology: devices and systems for room temperature operation* (John Wiley & Sons, 2015).
10. S. Preu, M. Mittendorff, H. Lu, H. Weber, S. Winnerl, and A. Gossard, "1550 nm ErAs:In(Al)GaAs large area photoconductive emitters," *Appl. Phys. Lett.* **101**, 101105 (2012).
11. H. Ito, F. Nakajima, T. Futura, and T. Ishibashi, "Continuous THz-wave generation using antenna-integrated uni-travelling-carrier photodiodes," *Semicond. Sci. Technol.* **20**, 191–198 (2005).
12. C. C. Renaud, M. Robertson, D. Rogers, R. Firth, P. J. Cannard, R. Moore, and A. J. Seeds, "A high responsivity, broadband waveguide uni-travelling carrier photodiode," *Proc. SPIE* **6194**, 6164C (2006).

13. E. Brown, A. Mingardi, W.-D. Zhang, A. Feldman, T. Harvey, and R. Mirin, "Abrupt dependence of ultrafast extrinsic photoconductivity on er fraction in GaAs:Er," *Appl. Phys. Lett.* **111**, 031104 (2017).
14. J. L. Hudgins, G. S. Simin, E. Santi, and M. A. Khan, "An assessment of wide bandgap semiconductors for power devices," *IEEE Trans. Power Electron.* **18**, 907–914 (2003).
15. R. A. Metzger, A. S. Brown, L. G. McCray, and J. A. Henige, "Structural and electrical properties of low temperature grown GaInAs," *J. Vac. Sci. Technol. B* **11**, 798–801 (1993).
16. D. C. Driscoll, M. P. Hanson, A. C. Gossard, and E. R. Brown, "Ultrafast photoresponse at 1.55 μm in InGaAs with embedded semimetallic ErAs nanoparticles," *Appl. Phys. Lett.* **86**, 051908 (2005).
17. J. Mangeney, N. Chimot, L. Meignien, N. Zerounian, P. Crozat, K. Blary, J. F. Lampin, and P. Mounaix, "Emission characteristics of ion-irradiated In_{0.53}Ga_{0.47}As based photoconductive antennas excited at 1.55 μm ," *Opt. Express* **15**, 8943–8950 (2007).
18. O. Hatem, J. Cunningham, E. Linfield, C. Wood, A. Davies, P. Cannard, M. Robertson, and D. Moodie, "Terahertz-frequency photoconductive detectors fabricated from metal-organic chemical vapor deposition-grown Fe-doped InGaAs," *Appl. Phys. Lett.* **98**, 121107 (2011).
19. B. Globisch, R. Dietz, R. Kohlhaas, T. Göbel, M. Schell, D. Alcer, M. Semtsiv, and W. Masselink, "Iron doped InGaAs: Competitive THz emitters and detectors fabricated from the same photoconductor," *J. Appl. Phys.* **121**, 053102 (2017).
20. B. Globisch, D. Stanze, R. J. Dietz, T. Gobel, and M. Schell, "Bandwidth improvement of CW THz receivers by Be doping of low-temperature-grown InGaAs/InAlAs heterostructures," in "Infrared, Millimeter, and Terahertz Waves (IRMMW-THz), 2013 38th International Conference on," (IEEE, 2013), pp. 1–2.
21. J. Suen, P. Krogen, S. Preu, H. Lu, A. Gossard, D. Driscoll, and P. Lubin, "Measurement and modeling of ErAs:In_{0.53}Ga_{0.47}As nanocomposite photoconductivity for THz generation at 1.55 μm pump wavelength," *J. Appl. Phys.* **116**, 013703 (2014).
22. I. S. Gregory, C. Baker, W. Tribe, M. Evans, H. E. Beere, E. H. Linfield, A. Davies, and M. Missous, "High resistivity annealed low-temperature GaAs with 100 fs lifetimes," *Appl. Phys. Lett.* **83**, 4199–4201 (2003).
23. D. C. Driscoll, M. Hanson, C. Kadow, and A. C. Gossard, "Electronic structure and conduction in a metal-semiconductor digital composite: ErAs:InGaAs," *Appl. Phys. Lett.* **78**, 1703–1705 (2001).
24. G. Segsneider, F. Jacob, T. Löffler, H. G. Roskos, S. Tautz, P. Kiesel, and G. Döhler, "Free-carrier dynamics in low-temperature-grown GaAs at high excitation densities investigated by time-domain terahertz spectroscopy," *Phys. Rev. B* **65**, 125205 (2002).
25. D. Driscoll, M. Hanson, C. Kadow, and A. C. Gossard, "Transition to insulating behavior in the metal-semiconductor digital composite ErAs:InGaAs," *J. Vac. Sci. Technol. B* **19**, 1631–1634 (2001).
26. J. D. Dyson, "The equiangular spiral antenna," *IRE Trans. Antenna Propag.* **7** 181–187 (1959).
27. A. J. Deninger, A. Roggenbuck, S. Schindler, and S. Preu, "2.75 THz tuning with a triple-DFB laser system at 1550 nm and InGaAs photomixers," *J. Infrar. Milli Thz Waves* **36**, 269–277 (2015).
28. M. T. Haidar, S. Preu, S. Paul, C. Gierl, J. Cesar, A. Emsia, and F. Küppers, "Widely tunable telecom MEMS-VCSEL for terahertz photomixing," *Optics Lett.* **40**, 4428–4431 (2015).

1. Introduction

The continuously growing market for Terahertz (100 GHz-10 THz) devices, systems and applications requires more powerful systems at lower cost. There are many ways to generate and detect Terahertz radiation, such as purely electronic devices [1–3], optical devices such as lasers [4] and mixed electronic and optical approaches such as photomixing [5]. Which approach is best suited depends on the application. For applications where large bandwidth, large tunability and good frequency resolution is required, continuous-wave (CW) photomixing is an excellent choice. Two lasers are detuned by the Terahertz frequency to be generated. The two tones are mixed by a semiconductor device that absorbs the heterodyned laser signal and generates a THz current at the difference frequency of the two. An attached antenna radiates the current as THz radiation. A particularly important type of photomixer is a photoconductor. It is a highly resistive semiconductor with low carrier lifetime that is switched by the laser to a lower resistance. An applied bias generates a THz current, following the resistance modulation, i.e. the laser envelope, oscillating at the difference frequency of the laser frequencies. CW photomixers require a very short carrier lifetime of the order of the inverse Terahertz frequency in order to allow the resistance to quickly switch back to the high resistive state, being able to follow the fast resistance modulation by the lasers. The tuning range depends on both the tuning range of the lasers, which can be several THz, and the bandwidth of the photomixers, which is in the range of 3-4 THz [6]. The frequency resolution is given by the linewidth of the lasers. Free running lasers typically

offer linewidths in the (sub-) MHz range, stabilized systems even allow for Hz-level linewidth [7]. Photoconductors are particularly relevant for photomixing systems because they can also be used as homodyne receivers by mixing the envelope signal of the heterodyned lasers and the received THz signal resulting in a DC photocurrent.

In the early days of photomixers, low temperature grown (LTG) GaAs photoconductors [8], operated with 800 nm lasers, dominated the photomixer market. The advent of 1550 nm wavelength telecommunication, however, makes systems operating at 1550 nm highly interesting since a large number of devices is available at lower cost than at 800 nm. Since the lasers are a major cost-factor of photomixing systems, nowadays 1550 nm operated systems are often preferred. While sources are often p-i-n diodes, photoconductors are usually the devices of choice for homodyne receivers because they offer excellent noise floors as low as a few ten fW/Hz. This combination allows for peak dynamic ranges of 80-100 dB even if the source produces only a few 10s of μW . However, photoconductive materials operating at 1550 nm are very difficult to design due to several, partially conflicting requirements. While a detailed theoretical description of photoconductors and their roll-offs can be found elsewhere [5, 9], the key parameters of CW photoconductors are summarized in the following:

- *High absorption at the laser wavelength*, ideally larger than 5000 /cm. This typically requires interband absorption and therefore materials with a band gap smaller than 0.8 eV for operation with telecom lasers [6, 10–12]. There are, however, a few examples in the literature where absorption via trap states located in the center of band gap allows for absorption of photons with approximately half the band gap energy [13]. This usually leads to somewhat lower absorption coefficients but may still be useful for Terahertz generation and detection if sufficient laser power is available.
- *High resistance under illumination*, R_{ill} , is required for detectors in order to reduce the noise floor. Since photoconductive detectors are current sources for the detection circuit, their thermal noise is given by

$$I_N^{PC} = \sqrt{4k_B T / R_{ill}}. \quad (1)$$

The resistance under illumination should at least be the equivalent noise input resistance of the post detection electronics, $R_N = (4k_B T) / (I_N^{TIA})^2$, where I_N^{TIA} is the input noise equivalent current of the post detection transimpedance amplifier. Though this ensures that the noise floor is only limited by the post detection electronics with no or little noise increase by the photoconductor, this condition is barely met under CW operation by any receiver. Further, a large resistance reduces the amount of current generated by stray fields in the laboratory and therefore reduce secondary noise effects. Sources require high resistance because they are DC biased. The DC bias causes additional DC current of $I_{DC} = U_{DC} / R_{ill}$ flowing through the device. This DC current is of no use for the THz amplitude but heats up the source and therefore limits the amount of laser power and maximum bias to be applied before thermal failure occurs. The illuminated device resistance should be several 10 k Ω under CW operation to reduce the impact of thermal limitations. The dark resistance typically has to be in the range of 1 M Ω or larger to reach such excellent resistances under illumination. High resistances are particularly difficult to engineer for low band gap materials since the intrinsic carrier concentration scales as $n_i \sim \exp[-eE_G / (2k_B T)]$, so does the dark conductivity. The high dark conductance is a major issue for telecom-wavelength compatible photoconductors with interband absorption such as InGaAs as compared to LTG GaAs which offers an about 2 times larger band gap.

- *Short carrier lifetimes* are required to ensure that the material can follow the THz modulation by the lasers. Ideally, the carrier lifetime should be $\tau_{rec} = (2\pi f_{3dB})^{-1}$ for a target 3 dB

frequency of f_{3dB} [5]. Above this frequency, the device efficiency falls off as f^{-2} for both sources and receivers.

- *High (AC) mobility*, μ , leads to large currents according to $I \sim \mu E_i$, where $E_i = E_{THz}$ for the receiver and $E_i = E_{DC}$ for sources, i.e. the accelerating DC field which is proportional to the DC bias.
- *Large break down field strength* is necessary for photoconductive sources because large biases are applied to the electrodes attached to the photoconductor in order to yield the largest possible THz current. High break down field strengths are particularly difficult to engineer for low band gap semiconductors since the break down field strength, E_{bd} , scales approximately with the band gap of the semiconductor, E_G , as $E_{bd} \sim E_G^{2.5}$ [14]. Good values for break down field strengths for photoconductors are above 100 kV/cm².

Unfortunately, these requirements usually cannot be maximized at the same time. For instance, a short carrier lifetime requires many efficient trapping centers, which also act as scatterers, reducing the mobility. There are several examples in the literature for 1550 nm photoconductors. In the early days of telecom-wavelength-compatible photoconductors, devices were fabricated from low temperature grown (LTG) InGaAs, lattice matched to InP [15]. Though short carrier lifetimes could be engineered, LTG-InGaAs features a strong n-type background since the Fermi energy is close to the conduction band edge. Similarly, ErAs inclusions in InGaAs result in an n-type background that requires strong p-doping for compensation [16], reaching carrier lifetimes in the range of 0.3 ps and sheet resistances of 400 Ω cm. Another approach uses ion-damaging of InGaAs [17]. Similarly, short carrier lifetimes of the order of 0.3 ps could be achieved but the devices were always fairly n-type with resistances in the range of 5 Ω cm only. Iron-doping of chemical vapor deposited InGaAs also faced heavy n-type conductivity at good values for the carrier lifetime at least for growth by chemical vapor deposition [18]. Material grown by molecular beam epitaxy seems to be better suited [19]. An approach that leads to high device resistance and short carrier lifetime at the same time is extrinsic photoconductivity in ErAs:GaAs, where ErAs forms a miniband in the band gap of GaAs [13]. While pulsed operation of such devices has yet been reported, there are no CW results in the literature so far. The so far most successful approach uses a superlattice of absorbing LTG InGaAs layers and LTG InAlAs, lattice matched to InP [6] with excellent carrier lifetimes in the range of 0.2-3.2 ps and, at the same time, high dark resistivity [20]. We have previously shown that a superlattice consisting of intrinsic InGaAs, ErAs and InAlAs results in excellent performance with mobilities in the range of 1400 cm²/Vs, resistances in the range of 670 Ω cm, and carrier lifetimes between 0.52 and 2.2 ps [10, 21]. These device parameters allowed for constructing efficient large area emitters with a bandwidth of greater than 3 THz [10]. Based on this approach, we show in this paper ErAs:InGaAs homodyne detectors and ErAs:In(Al)GaAs photoconductive THz sources with excellent device parameters and THz performance under CW operation.

2. The ErAs:In(Al)GaAs material system

The ErAs:In(Al)GaAs photoconductors consist of a superlattice layer structure as depicted in Fig. 1. It should be noted that none of the used materials is a low lifetime material. Only the combination of the layers creates the desired parameters. The detector material is illustrated in Fig. 1 (a). It consists of a superlattice of intrinsic InGaAs and 0.8 monolayers (ML) of delta-p-doped semi-metallic ErAs. The superlattice material is grown at the optimum growth temperature of InGaAs around 490°C. Therefore, high crystalline quality is achieved, even for a large number of superlattice periods [16]. Since InGaAs grows in the Zinkblende crystal structure but ErAs in the Wurzite structure, ErAs is non-wetting and clusters automatically without the requirement of a subsequent annealing step as for LT-GaAs and LT-InGaAs [22].

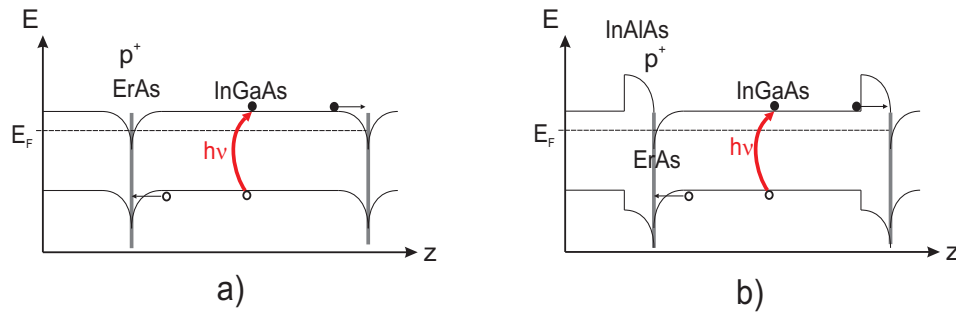


Fig. 1. a) 1.5 periods of the material structure of the receivers. b) 1.5 periods of the layer sequence of the photoconductive source. The delta-doping of all samples is in the range of a few $10^{13}/\text{cm}^2$.

Clustering allows for excellent overgrowth starting at exposed InGaAs if the ErAs thickness is below ~ 2.4 ML [23]. ErAs is excellently suited for carrier trapping because it is a semi-metal with a huge number of available trap states, much larger than that of As-clusters in LT-GaAs or LT-InGaAs which is of the order of a few 10^{18} cm^{-3} only [24]. Similar to LT-InGaAs, ErAs features a Fermi level close to the conduction band of InGaAs [25], therefore introducing an n-type background. In contrast to low-temperature grown InGaAs the position along the growth direction and the size of the ErAs clusters can be well defined during growth. This allows for accurately compensating the n-background by delta-doping around the ErAs clusters. Both ErAs and InGaAs growth are under excellent control, allowing for fairly high reproducibility. The thickness of the InGaAs layer, d_{InGaAs} is chosen sufficiently short to ensure sub-ps diffusion and drift times of the optically generated carriers to the trapping ErAs clusters. The average diffusion time is the lower limit of the carrier lifetime to be expected for this material and are reached if the trapping efficiency of the clusters is unity. We have chosen $d_{\text{InGaAs}}=10$ nm for the receivers and $d_{\text{InGaAs}}=15$ nm for the source. Experimentally, a (zero bias) carrier lifetime of the receiver of 520 fs and 1.3 ps of the source has been determined [21], in excellent agreement with values found in [16]. When implemented as source, the diffusion time may be shorter due to the applied DC bias, pushing the charge carriers towards the ErAs clusters. For THz photoconductive sources, we implement the design shown in Fig. 1 (b). In addition to the intrinsic InGaAs layer and p-doped ErAs, an additional 2.5 nm InAlAs layer is included in the superlattice structure in order to increase the break down field strength. The break down field strength under dark conditions of the source superlattice structure is 170 ± 40 kV/cm, determined from dark IV characteristics on separate devices. To the knowledge of the authors, this is the largest break down field strength reported so far for InGaAs-based photoconductors. Under illumination and biasing, spatial separation and subsequent trapping of the optically generated carriers leads to charging of the contact electrodes [9]. The local fields close to the electrodes are therefore larger than the average field, U_{DC}/w_G , where U_{DC} is the applied DC bias and w_G is the distance of the electrodes, while the field in the center between the electrodes is smaller. The larger local field strength in the vicinity of the electrodes decreases the maximum applicable bias. Further, the photocurrent and bias generate heat which may drive the photoconductor into its thermal limit at high biases. The strength of both effects depend on several parameters, such as the carrier lifetime, the electrode separation and the Fermi-pinning of the semiconductor as compared to the metal. For the photoconductive sources presented here ($w_G = 1.9 \mu\text{m}$, $\tau_{\text{rec}}=1.3$ ps), the break down field strength/maximum bias field at 26 mW laser power decreases to about 47 kV/cm which is sufficient for high dynamic range THz systems. The carrier lifetime of the receivers used in this publication is about 0.52 ps. The key parameters of the photoconductors are summarized

in table 1. The absorption coefficient of the receiver is identical to that of intrinsic InGaAs within the measurement error. The source shows a slightly smaller absorption coefficient due to quantum confinement. The receivers feature 100 superlattice periods shown in Fig. 1 (a) with a total a thickness of $1 \mu\text{m}$, resulting in 53% absorption at 1550 nm. The source superlattice uses 70 periods of the layer sequence shown in Fig. 1 (b) with a total thickness is $1.225 \mu\text{m}$, thereof $1 \mu\text{m}$ InGaAs absorbing about 50 % of the incoming optical signal at 1550 nm, respectively, leaving plenty of room for improvement in terms of reduction of laser power by larger absorption with thicker structures for both source and receiver.

Table 1. Summary of the key parameters of the fabricated photoconductors.

	τ_{rec} [ps]	R_{dark} [M Ω]	R_{ill} [k Ω] at 26 mW	Absorption, 1550 nm
Receiver 1	0.53 ± 0.05	0.3 ± 0.03	5.6 ± 0.6	53 %
Receiver 2	0.52 ± 0.05	0.13 ± 0.01	5.6 ± 0.6	53 %
Source	1.7 ± 0.4	4.5 ± 0.8	29 ± 3	50 %

The photoconductors use an interdigitated finger structure with a finger width of $1.1 \mu\text{m}$ and a gap of $w_G = 1.9 \mu\text{m}$ as depicted in the inset of Fig. 2. The fingers are defined using UV contact lithography only, i.e no electron beam lithography is required. The photocurrent is fed into a broadband logarithmic spiral antenna with a radiation resistance of 70Ω , designed for frequencies between 50 GHz and about 1.5-2 THz. Outside this operation range, the antenna still emits radiation fairly well, however, the polarization changes from circular to elliptic [26] and the radiation resistance deviates from 70Ω .

3. CW THz spectroscopy system using only ErAs:In(Al)GaAs devices

Though CW 1550 nm Terahertz systems usually use p-i-n diode based sources, we demonstrate the strength of the material system by employing ErAs-based photoconductors as both source and receiver (receiver 1 in table 1). The laser power for driving both photoconductors is $26 \pm 2 \text{ mW}$ each, the source is bias-modulated from -7.5 V to 7.5 V for lock-in detection. Prior to lock-in detection, the received photocurrent is preamplified using a PDA-S transimpedance amplifier (TEM Messtechnik) at 10^6 V/A . The devices are attached to logarithmic spiral antennas and mounted on hyperhemispheric silicon lenses. Two TPX lenses propagate the THz power from source to receiver. The system does not use any delay lines. The amplitude information is extracted from one oscillation in the frequency domain with a period of 563 MHz by using different path lengths for receiver and source laser path. Figure 2 shows the dynamic range up to 2.75 THz, which is the maximum frequency permitted by the used laser system, for a lock-in time constant of 300 ms. The peak dynamic range is 78 dB at 123 GHz. At 1 THz we achieve 52 dB dynamic range, at 2 THz 31.7 dB and at the maximum frequency of the laser system of 2.75 THz, the dynamic range is still $16.4 \pm 0.1 \text{ dB}$. Following the trend of the power vs. frequency, the maximum operation frequency of the system is expected to be around 3.65 THz. To the knowledge of the authors, this is the highest dynamic range and the largest bandwidth of a system only using 1550 nm compatible photoconductors.

The measured THz photocurrent at the receiver (the DNR) increases linearly (quadratically) with source DC bias without any noticeable saturation within the examined biasing range. Therefore, the dynamic range can further be improved by using larger biases at the source. The data shown use a peak amplitude of 7.5 V , however, the ErAs:In(Al)GaAs source withstood also a biasing of 9 V under illumination. The source finally broke at 9.5 V . Unfortunately, we did not record any spectra at a bias of 9 V . The bias of 7.5 V can be considered as a safe bias for long term operation.

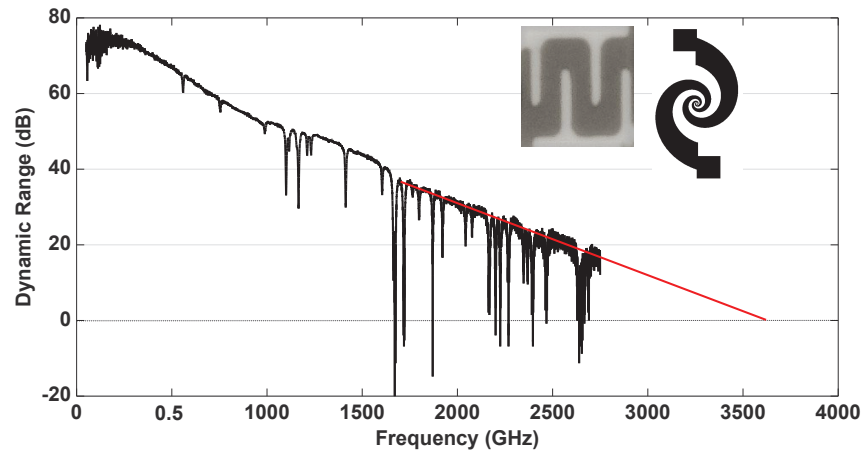


Fig. 2. Dynamic range of a system using only ErAs:In(Al)GaAs photoconductors. The source is biased at ± 7.5 V at 12.2 kHz, being a safe bias for long-term operation. The insets show the used spiral antenna and an image of the electrode structure. The photoconductive gap (i.e. the finger spacing) for all devices is $w_G = 1.9 \mu\text{m}$ using 2 fingers of length $7.1 \mu\text{m}$ and width $1.1 \mu\text{m}$ on each electrode, covering a total area of $10 \times 10 \mu\text{m}^2$.

4. ErAs:InGaAs receiver characterization

Photoconductors are required for all homodyne systems as receivers, in particular also for high dynamic range systems using p-i-n diode based sources [6]. Therefore, the receiver performance deserves a closer look. The (power) noise floor is inversely proportional to the integration time as expected for a homodyne system, confirmed by recording the noise with the THz path blocked by Aluminum foil for integration times of 3 ms, 30 ms, and 300 ms. The responsivity of the receiver is linear with the laser power up to the maximum available laser power of 27.8 mW. Figure 3 shows both the dynamic range at a source bias of 5.2 ± 0.2 V and the current noise floor of the receiver vs. laser power at 1 THz, calculated for 300 ms integration time. The difference in terms of noise to a measurement with a source bias of 7.5V is very marginal, showing little electrical cross talk between the bias path and the post detection electronics on the receiver side. The current noise is limited by the system noise of 1.9 pA and roughly linearly increases within the examined power range. The reason for the linear increase is a superlinear increase of the photoconductivity with laser power which requires further investigations. The dynamic range of the system shows a saturation behavior and reaches its saturation DNR of 37.7 ± 0.2 dB at a laser power of 12 mW allowing to drive the receiver even at lower power levels than used in the THz experiments. The noise current is 5.47 pA at $\tau = 300$ ms integration time constant at 12 mW being very similar to commercial devices (5 pA in the subsequent section) and increases to 10.95 pA at the full laser power of 26 ± 1 mW. The noise equivalent power (NEP) of the receiver is determined using a Golay cell as reference power meter to 19 fW/Hz at 1 THz, assuming a lock-in $ENBW = 1/(2\tau)$ as specified by Toptica.

5. Receiver comparison to commercial device

For comparing an ErAs:InGaAs receiver to the state of the art, we use a Toptica photonics photomixing system with source and receiver from the Fraunhofer Heinrich Hertz institute and three DFB diodes to cover a spectral range of 50 GHz-2.75 THz, identical to that shown in [27]. The only difference is a slightly lower source bias and slightly lower laser power in order to increase the source lifetime. The THz path uses two parabolic mirrors and two TPX lenses

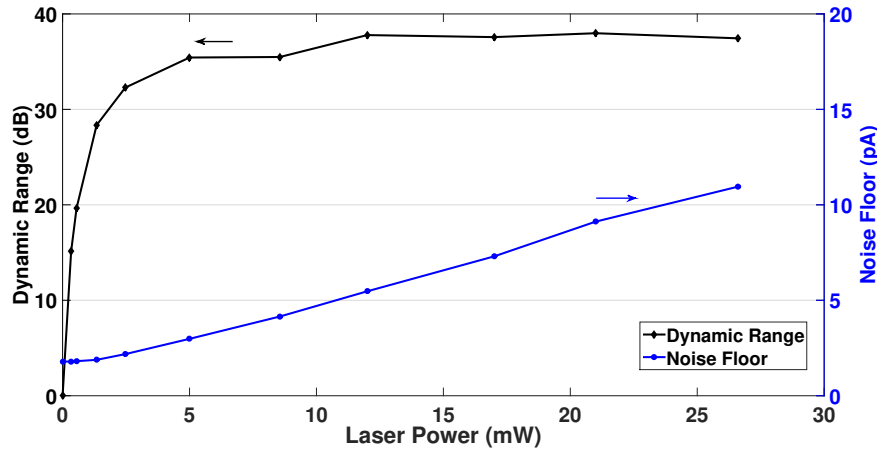


Fig. 3. Noise floor of the receiver and dynamic range of the system at 1 THz, 300 ms integration time, and 5.2 ± 0.2 V source voltage amplitude vs. laser power.

between the parabolas. For noise measurements, the system was kept running and the THz beam was blanked by a metal shield. The source and receiver of the commercial system use linearly polarized antennas, while the ErAs:InGaAs receiver is attached to a spiral antenna with circular polarization. The ErAs:InGaAs receiver (receiver 2) implemented in this measurement is a device from a different wafer than that used in the previous experiment, however, with nominally the same structure and comparable performance, proofing the reproducibility of the sample quality. The only difference is Carbon-doped ErAs instead of Be-doped ErAs. Figure 4 shows a comparison of the commercial system to the system with the commercial receiver replaced by the ErAs:InGaAs photoconductor at an integration time of 30 ms. The ErAs:InGaAs receiver shows better performance all across the investigated spectral range, except at low frequencies, where the commercial and the ErAs:InGaAs receiver perform about the same. At frequencies above 1 THz, the ErAs:InGaAs receiver offers about 3 dB larger dynamic range (DNR) despite the mismatch of the antenna types and polarisations (i.e. 3 dB loss within the operation range of the spiral antenna). Therefore, the NEP is a factor of 2 lower than that of the commercial receiver. If identical antennas were used, the NEP would be 4 times lower due to increased responsivity.

The extrapolated bandwidth of the system with the ErAs:InGaAs receiver of 3.45 THz is slightly larger than the system using both commercial source and receiver (3.3 THz), while the system using only ErAs:In(Al)GaAs-based photomixers offers 3.65 THz. Above 2 THz, the DNR with the commercial system under these driving conditions is already smaller than the DNR of the system using only ErAs-based photoconductors in Fig. 2. Even under maximum operation conditions of the commercial p-i-n-diode based source as shown in [27], an (extrapolated) bandwidth of 3.5 ± 0.1 THz can be expected, being still smaller than that of the ErAs:In(Al)GaAs based photomixer system in Fig. 2. We therefore conclude that the ErAs:InAlGaAs-based photoconductive source is competitive with the p-i-n diode based commercial device at high THz frequencies, offering larger bandwidth at cost of lower dynamic range at low frequencies. The improved bandwidth is mainly due to a less severe lifetime roll-off ($f_{3dB}^T = (2\pi\tau_{rec})^{-1} \approx 305 GHz$) and less severe RC roll-off of the photoconductor with a simulated capacitance of 3.7 ± 0.2 fF, yielding a 3 dB frequency of 0.61 THz for a 70Ω radiation resistance.

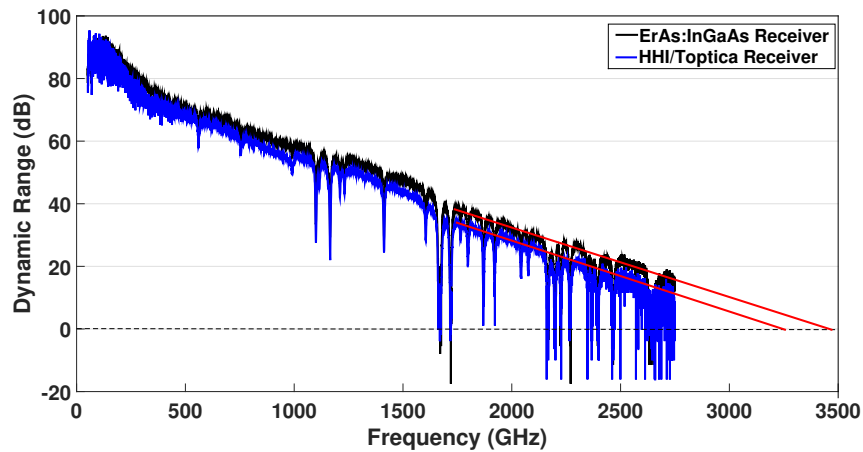


Fig. 4. Comparison of the system using the commercial receiver (blue) and that with the commercial receiver replaced by the ErAs:InGaAs receiver 2 (black).

6. Conclusions and outlook

To the knowledge of the authors, 52 dB (31.7 dB) at 1 THz (2 THz) is the highest dynamic range reported for a CW system operating at 1550 nm using only photoconductive elements. The extrapolated bandwidth of 3.65 THz is on the level of the largest bandwidths reported to date with any 1550 nm CW THz system. There is still large room for improvement, e.g. by optimized electrode structures with reduced capacitance or enhanced optical responsivity by using electron beam lithography, larger optical power levels, and improved antenna designs extending the operation range towards higher frequencies. These steps will further improve both the dynamic range and bandwidth of the presented systems. The devices are operated with commercial DFB laser diodes without the requirement of amplifiers. The receiver NEP saturates at 12 mW already. Since the devices absorb only 50-53% of the laser power, samples with increased absorber thickness will lead to even lower saturation powers and lower powers required to drive the source. This improves the optical to THz conversion efficiency and allows implementation in laser systems with enhanced bandwidth or compactness that are usually discarded because of smaller available laser powers, such as VCSEL-based systems [28].

Funding

Deutsche Forschungsgemeinschaft (DFG), project “REPHCON” PR1413/3-1; European Union Horizon 2020 Marie Skłodowska Curie actions, innovative training network (ITN) “CELTA” Grant No. 675683.